

The cosmic assembly of stellar haloes in massive Early-Type Galaxies

Fernando Buitrago^{1,2,3} ^{*}, Ignacio Trujillo^{4,5}, Emma Curtis-Lake^{1,6}, Mireia Montes⁷, Andrew P. Cooper⁸, Victoria A. Bruce¹, , Pablo G. Pérez-González⁹, Michele Cirasuolo¹⁰

¹*SUPA†, Institute for Astronomy, University of Edinburgh, Royal Observatory, Edinburgh, EH9 3HJ, U.K.*

²*Instituto de Astrofísica e Ciências do Espaço, Universidade de Lisboa, OAL, Tapada da Ajuda, PT1349-018 Lisbon, Portugal*

³*Departamento de Física, Faculdade de Ciências, Universidade de Lisboa, Edifício C8, Campo Grande, PT1749-016 Lisbon, Portugal*

⁴*Instituto de Astrofísica de Canarias, Vía Láctea s/n, 38200 La Laguna, Tenerife, Spain*

⁵*Departamento de Astrofísica, Universidad de La Laguna, E-38205, La Laguna, Tenerife, Spain*

⁶*Sorbonne Universités, UPMC-CNRS, UMR7095, Institut d'Astrophysique de Paris, F-75014, Paris, France*

⁷*Department of Astronomy, Yale University, New Haven, CT 06511, USA*

⁸*Institute for Computational Cosmology, Durham, UK*

⁹*Departamento de Astrofísica, Facultad de CC. Físicas, Universidad Complutense de Madrid, E-28040 Madrid, Spain*

¹⁰*European Southern Observatory Karl-Schwarzschild-Strasse 2, D-85748 Garching bei Muenchen, Germany*

6 March 2022

ABSTRACT

Using the exquisite depth of the Hubble Ultra Deep Field (HUDF12 programme) dataset, we explore the ongoing assembly of the outermost regions of the most massive galaxies ($M_{\text{stellar}} \geq 5 \times 10^{10} M_{\odot}$) at $z \leq 1$. The outskirts of massive objects, particularly Early-Type Galaxies (ETGs), are expected to suffer a dramatic transformation across cosmic time due to continuous accretion of small galaxies. HUDF imaging allows us to study this process at intermediate redshifts in 6 massive galaxies, exploring the individual surface brightness profiles out to ~ 25 effective radii. We find that 5-20% of the total stellar mass for the galaxies in our sample is contained within $10 < R < 50$ kpc. These values are in close agreement with numerical simulations, and higher than those reported for local late-type galaxies ($\lesssim 5\%$). The fraction of stellar mass stored in the outer envelopes/haloes of Massive Early-Type Galaxies increases with decreasing redshift, being 28.7% at $\langle z \rangle = 0.1$, 15.1% at $\langle z \rangle = 0.65$ and 3.5% at $\langle z \rangle = 2$. The fraction of mass in diffuse features linked with ongoing minor merger events is > 1 -2%, very similar to predictions based on observed close pair counts. Therefore, the results for our small albeit meaningful sample suggest that the size and mass growth of the most massive galaxies have been solely driven by minor and major merging from $z = 1$ to today.

Key words: galaxies: evolution – galaxies: high-redshift – galaxies: morphology – galaxies: elliptical and lenticular, cD – galaxies: haloes – galaxies: structure

1 INTRODUCTION

There is ample evidence that the most massive galaxies of the Universe have grown dramatically in size since $z = 3$ (Daddi et al. 2005; Trujillo et al. 2006a,b; Toft et al. 2007; Cimatti et al. 2008; Buitrago et al. 2008; Damjanov et al. 2009; van Dokkum et al. 2010; Cassata et al. 2011; Bell et al. 2012; Bruce et al. 2012; Huertas-Company et al. 2013, to name but a few). Early-

Type Galaxies (ETGs) –selected by their morphological classification, or through a proxy like colours or quiescent star formation– are those that display the most extreme evolution (with sizes ~ 5 times smaller on average, at a given stellar mass, than their local Universe counterparts; Trujillo et al. 2007; Buitrago et al. 2008; van der Wel et al. 2014).

Theoretically, massive galaxies are predicted to undergo a two-phase formation process whereby there is a initial very rapid and dissipative gas collapse at high- z where most of the in-situ stars originate (Khochfar & Silk (2006); Oser et al. (2010); Ceverino et al.

^{*} E-mail: fbuitrago@oal.ul.pt

[†] Scottish Universities Physics Alliance

(2015); Zolotov et al. (2015); Wellons et al. (2016), see observations in Ricciardelli et al. (2010); Barro et al. (2013); Huang et al. (2013); Williams et al. (2014) as well). The next stage must be a combination of major and minor mergers (Bezanson et al. 2009; Hopkins et al. 2009; Ferreras et al. 2014; Xie et al. 2015), as these processes best reproduce the observed tight scatter in the size-mass relation of massive galaxies, and can account for the only mild mass increase in these systems from high redshift to the present day. In this context, some growth is also expected from residual star formation (Pérez-González et al. 2008a; Fumagalli et al. 2014). As a consequence, galaxies progressively build up their outer parts (aka galactic outskirts or outer stellar envelopes) and thus grow in an inside-out fashion (van Dokkum et al. 2010; Trujillo et al. 2011; Buitrago et al. 2013).

Many observational problems prevent us from directly testing the aforementioned scenario. First, the outskirts of galaxies are intrinsically the faintest parts of these systems. Secondly, surface brightness dimming rises very steeply by $(1+z)^3$ (see Giavalisco et al. 1996; Ribeiro et al. 2016). Therefore, if these studies are extremely challenging in the local Universe, conducting them at high redshift has been regarded as unfeasible.

Various techniques have been applied in order to overcome these hurdles in the local Universe and to extract the information enclosed in the outer regions of massive galaxies. These include: stacking (Zibetti et al. 2004; Tal & van Dokkum 2011; La Barbera et al. 2012; D’Souza et al. 2014), deep photometric studies (Zibetti & Ferguson 2004; Atkinson et al. 2013; van Dokkum et al. 2014; Duc et al. 2015; Trujillo & Fliri 2016), very deep spectroscopic analyses (Coccato et al. 2010) or stellar counts (Crnojević et al. 2013; Rejkuba et al. 2014). In doing so we have learned that $\sim 70\%$ of the nearby massive ETGs show features indicative of mergers or the tidal disruption of less massive companions (van Dokkum 2005; Tal et al. 2009; Kaviraj 2010). The observed features, such as shells or tidal tails, are red, smooth and extended (sometimes > 50 kpc). This has led to an overall consensus that these galaxies are assembled via mergers involving gas-poor and bulge-dominated systems.

The new observations of the Hubble Ultra Deep Field (HUDF), in particular the HUDF12 programme (Ellis et al. 2013; Koekemoer et al. 2013), have opened up the possibility of exploring galaxies to an unprecedented level of detail (5σ limiting magnitude ~ 30 AB mag). The extraordinary depth and resolution of these observations, combined with the fact that HUDF12 is the only HUDF programme which preserves the galaxy extended envelopes/haloes, enable us to study galaxy surface brightness profiles down to 31 mag arcsec $^{-2}$ or 25 effective radii (r_e) for the galaxies in our sample, sometimes reaching ~ 100 kpc in galactocentric distance.

In the present paper we perform an investigation on the nature of the galaxy outskirts at large galactocentric distances in these ETGs, trying to understand their observables (e.g. percentage of light and mass with respect to the central parts, colours, mass profiles), focusing our study on constraining the mass assembly of massive galaxies, giving the first, direct measurement of the mass growth by ongoing mergers.

The structure of the paper is as follows: Sections 2, 3

and 4 present the data, the sample and the analysis respectively. Section 5 shows the several tests we carried out for describing the stellar haloes in our sample of massive galaxies and finally, Section 6 delivers our summary and conclusions. Hereafter, we adopt a cosmology with $\Omega_m=0.3$, $\Omega_\Lambda=0.7$ and $H_0=70$ kms $^{-1}$ Mpc $^{-1}$. We use a Chabrier (2003) Initial Mass Function (IMF), unless otherwise stated. Magnitudes are provided in the AB system (Oke & Gunn 1983).

2 THE DATA

We analyzed the deepest ever HST observations, the Hubble Ultra Deep Field (HUDF; R.A. = 03:32:39.0, DEC = - 27:47:29.1, J2000). In order to detect extended stellar haloes around intermediate-redshift galaxies, the best Near-Infrared (NIR) data available was provided by the HUDF12¹ programme (Ellis et al. 2013; Koekemoer et al. 2013). This survey combines the images from the HUDF09 programme (Bouwens et al. 2012, and references therein) with a new 128-orbit campaign (HST Program ID 12498, PI.: R. Ellis and R. McLure). This translates into an outstanding improvement of the previous dataset, by enhancing the exposure times (sometimes even quadrupling them, as for the F105W filter) and adding new imaging in the F140W filter. Additionally, and key for our purposes, HUDF12 is unique as its HUDF data reduction preserves the faint wings of extended sources. Finally, in order to obtain the largest multiwavelength HST coverage, we also make use of the optical ACS observations² over the same area (Beckwith et al. 2006). Therefore, we have investigated the area (4.7 arcmin 2) where WFC3 and ACS observations overlap. We list the photometric bands, total exposure times and zeropoints in Table 1.

We also need to understand whether the level of background fluctuations in these data enables us to characterize very faint surface brightness features. We conducted a thorough characterization of each science image by placing 25000 random square 1×1 arcsec apertures in empty sky patches, inferring a surface brightness limit of ≥ 31 mag arcsec $^{-2}$ (only slightly brighter for Z-band) at a 3σ level over the background fluctuations in 10×10 arcsec boxes. The WFC3/IR images have passed multiple checks regarding their sky background properties, especially about persistence and large-scale flatfield variations. After the applied residual corrections, the sky is flat to within $\sim 1\text{--}2\%$ of mean sky level, translating into uniform limiting depths (≤ 0.03 mag) throughout the images. On the other hand, as it has been already indicated, the ACS programme targeting the HUDF is prior to the HUDF12 campaign, which is actually an asset to minimize the charge transfer efficiency degradation caused by radiation damage. It is to note that careful flatfielding and treatment of the scattered light was undertaken, as described at length in the Section 3.1 in Beckwith et al. (2006). The final residual flux is also $< 2\%$ of the sky level.

¹ <http://archive.stsci.edu/pub/hlsp/hudf12/>

² <http://archive.stsci.edu/pub/hlsp/udf/acs-wfc/>

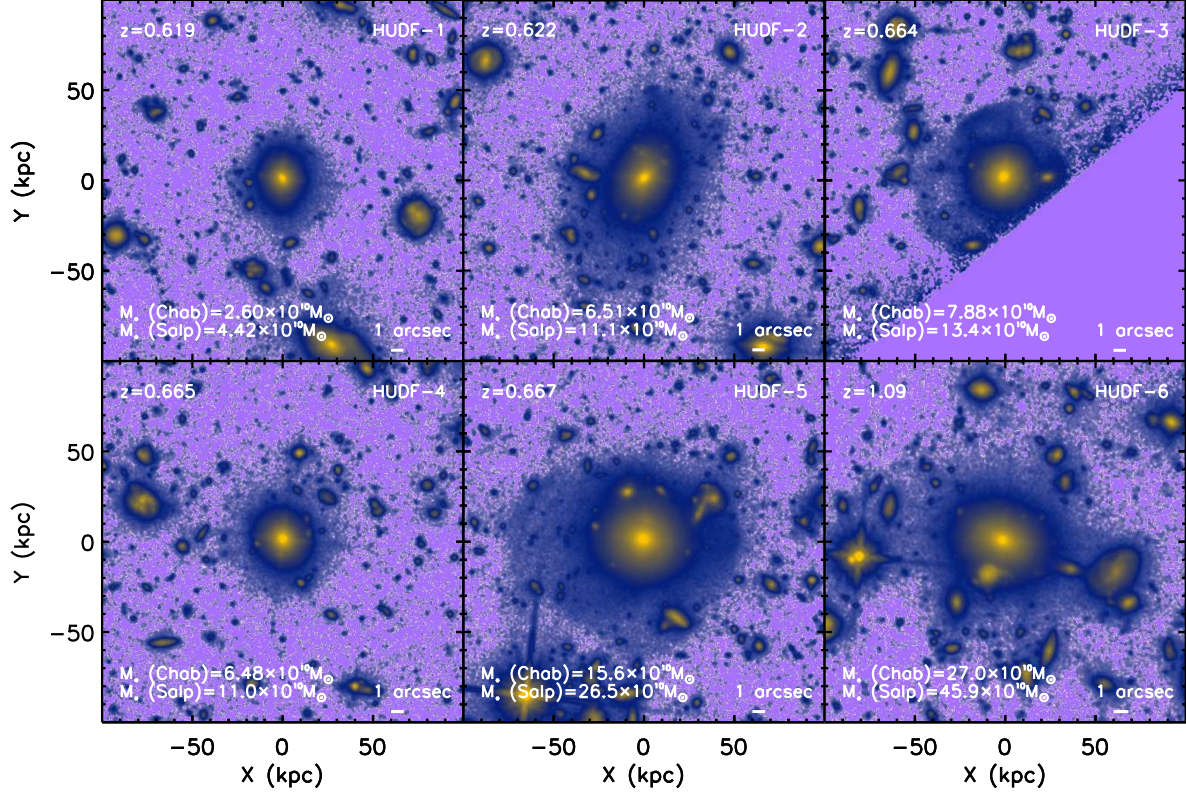


Figure 1. Montage with the HUDF12 WFC3 images for our sample of massive ETGs, also showing their spectroscopic redshifts and photometric masses. These are the stacked HST NIR images, and the colour palette ranges from 18 to 30 mag arcsec². The superb WFC3 resolution (approximately 0.18 arcsec, ~ 1.25 kpc at $\langle z \rangle = 0.65$, the median redshift of our observations) allow us to see the huge stellar envelopes for these objects, apart from broad fans of stars or shells (for HUDF-3 and HUDF-5) and other asymmetries. It is also striking the presence of so many potential satellites, which may contribute to the size increase of the massive objects via minor merging.

3 THE SAMPLE

The criteria for our galaxy selection are the following: ETG visual morphology, $M_{\text{stellar}} > 5 \times 10^{10} M_\odot$ and $z_{\text{spec}} \lesssim 1$ (to avoid severe cosmological dimming effects). We find 6 objects satisfying these criteria. These galaxies are also the most massive within the HUDF up to this redshift limit. Our galaxy sample was firstly identified by means of the Rainbow database³ (Pérez-González et al. 2008b; Barro et al. 2011a,b).

Spectroscopic redshifts are available for our whole sample (Croom et al. 2001; Vanzella et al. 2005; Le Fèvre et al. 2005; Ravikumar et al. 2007). In order to be self consistent and to use the information in the HUDF images, instead of using the Rainbow mass estimates, we performed SED fitting using the Le Phare photometric redshift code (Arnouts et al. 1999; Ilbert et al. 2006) to obtain stellar masses for each object based on the the total fluxes derived from the 4 Sérsic component fits plus residuals (see

Section 4.1). A range of short duration tau models (30, 70, 100, 300 Myr e-folding time) and a burst model were included in the template set. The models were produced using Bruzual & Charlot (2003) (BC03) at solar metallicity with a Chabrier (2003) IMF. The fitted ages were required to be younger than the age of the Universe at the redshift of the source, and no dust extinction was allowed in the fitting, because it is expected to be of negligible importance for massive ETGs. The outcomes for our galaxy sample are listed in Table 2.

We also supplement the table with the masses changed to a Salpeter (1955) IMF (+0.23 dex, as in Cimatti et al. (2008)) due to increasing evidence for a more bottom-heavy IMF for massive galaxies (La Barbera et al. 2013; Ferré-Mateu et al. 2013; Martín-Navarro et al. 2015). We stress that, according masses derived with a Chabrier IMF, HUDF-1 falls below our mass cut. However, given that the mass derived with a Salpeter IMF does meet our criteria, we chose to keep this object in our sample as it is among the most massive objects in HUDF at $z < 1$.

A montage with the galaxies in our sample is shown in

³ <https://rainbowx.fis.ucm.es/>

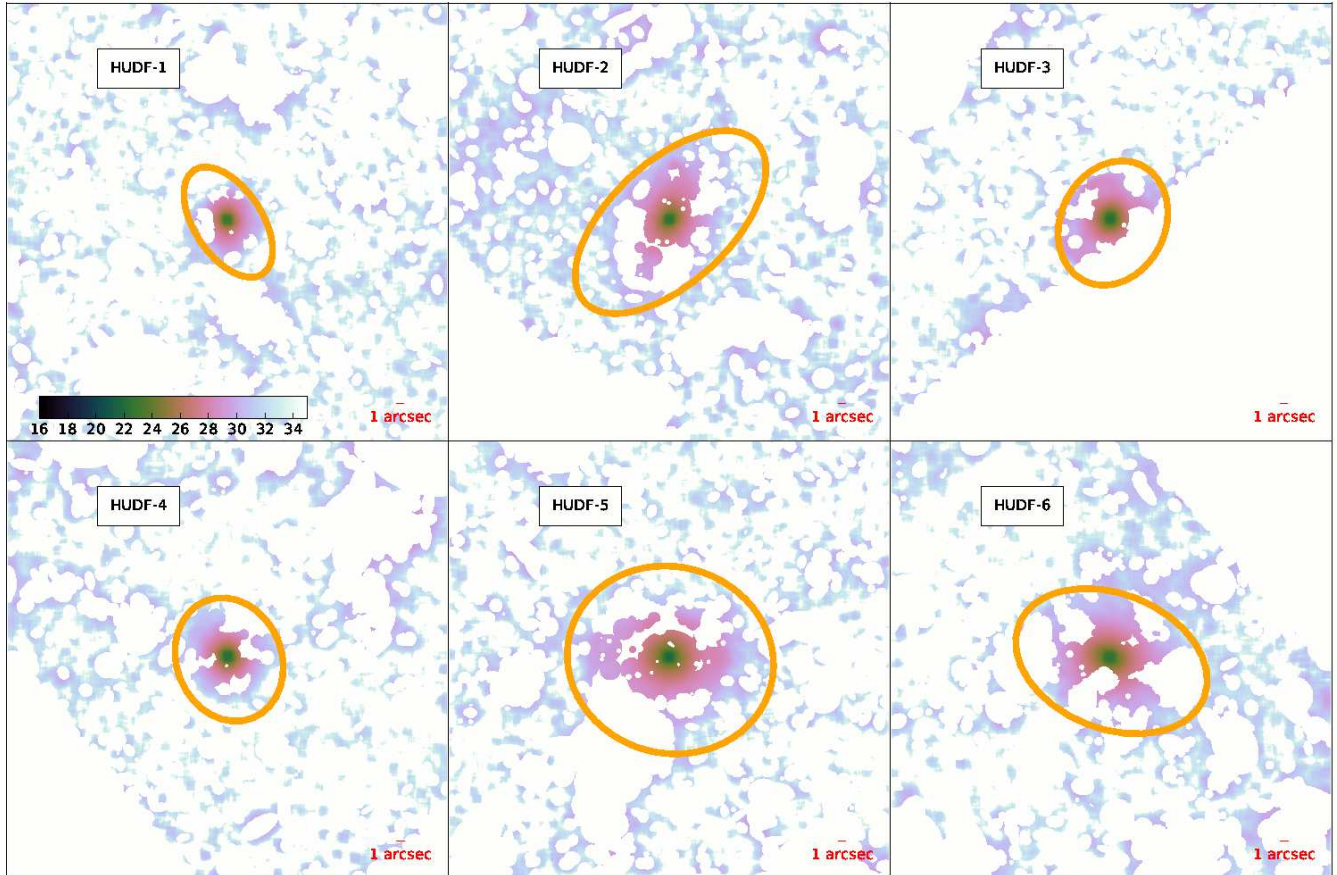


Figure 2. Coaddition of all near-infrared WFC3 images. The resulting image has been smoothed by convolving a 2-arcsec standard deviation Gaussian kernel and then our NIR mask of the galaxy neighbours has been overplotted. The whole process is done in order to highlight the lowest signal-to-noise features in the image. The colorbar displays the surface brightness in units of mag arcsec^{-2} . The golden ellipse shows the extent of our surface brightness analysis in the H-band (reddest band in the NIR).

Figure 1. The ubiquity of morphological low surface brightness features displayed by these galaxies is noteworthy (like the shells in HUDF-3 or the fan of stars in HUDF-5). In addition, a large number of minor objects surrounding the massive galaxies are present. It is beyond the scope of this paper to identify them as galactic satellites, but we would expect to see a large number of satellites if minor merging is significantly contributing to the evolution of massive galaxies (Bluck et al. 2012; Newman et al. 2012; López-Sanjuan et al. 2012; Mármol-Queraltó et al. 2012, 2013; Ferreras et al. 2014; Ruiz et al. 2015).

4 THE ANALYSIS

The survey images were carefully reduced and sky-subtracted (Koekemoer et al. 2013). We created 400 kpc wide postage stamps to explore the light distribution around the galaxies in the 8 filters available. We masked the neighbouring objects using SExtractor-based (Bertin & Arnouts 1996) optical and NIR masks, which were later visually in-

spected and modified to remove any spurious light contribution. The final depictions of our masks upon the galaxy images are shown in Figures 2 and 3. The displayed images are the coaddition of all NIR and optical bands and they have also been smoothed by a 2-arcsec standard deviation Gaussian kernel. These choices have been taken in order to highlight the lowest signal-to-noise features in the images. It is also fair to say that, despite the generous masking that has been applied, it is impossible to get rid of every single source of contamination. Nevertheless, after this careful effort, all the massive galaxies steadily decrease their surface brightness profiles down to the detection limits (golden ellipses).

We also require very accurate local sky subtraction as any residual background hampers our efforts for exploiting the extraordinary depth of our imaging. This aspect is particularly relevant if one is to sample very faint surface brightness features, and we proceeded as in Trujillo & Bakos (2013). We determined that the sky noise was dominant at galactocentric distances higher than 120 kpc for all galaxies. Therefore, we estimated the sky level in each image at a radial distance of $140 < R < 160$ kpc and subtracted that value. This meticulous analysis enables us to detect galaxy light down to $31 \text{ mag arcsec}^{-2}$ (3σ in $10 \times 10 \text{ arcsec}$ boxes),

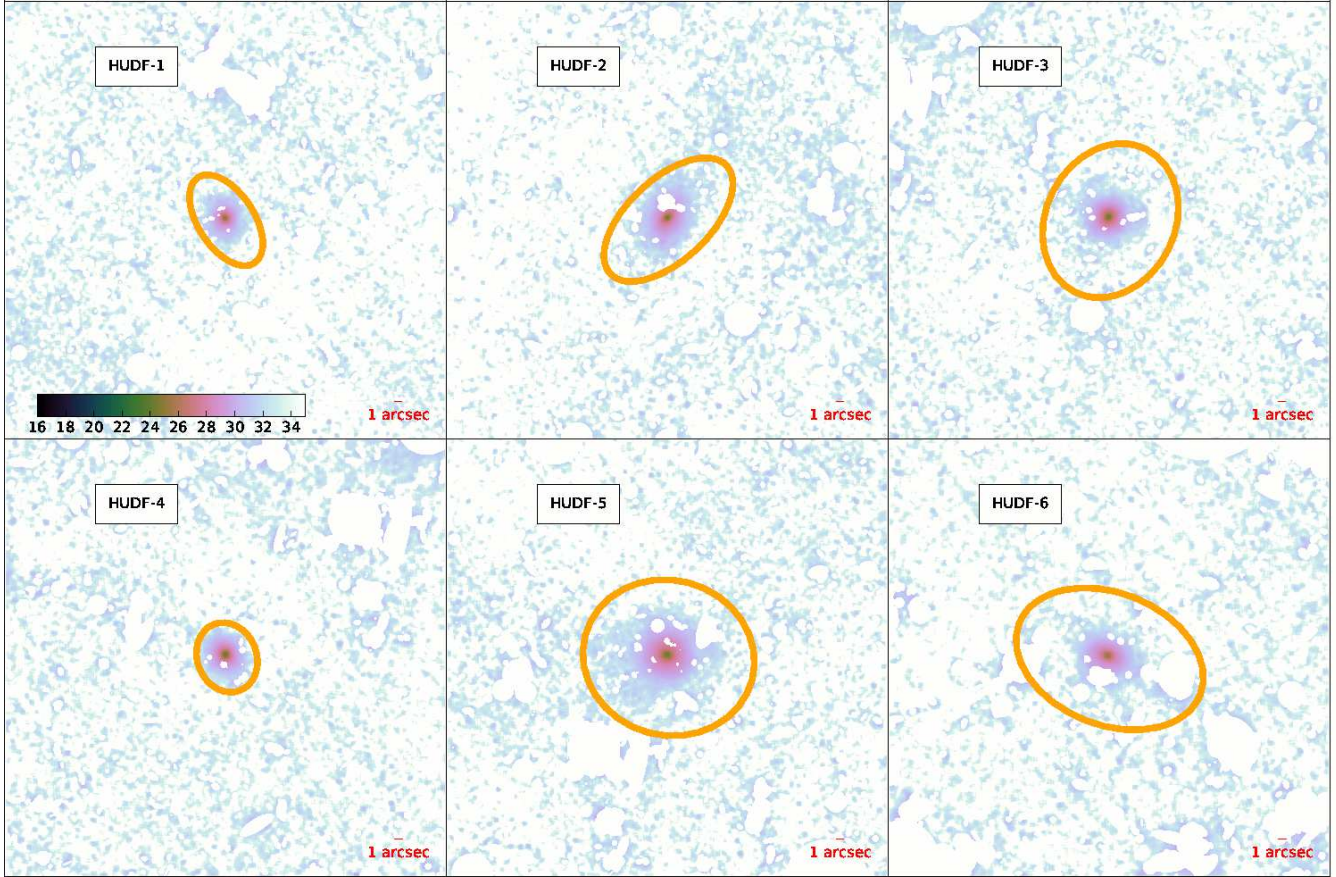


Figure 3. Coaddition of all optical ACS images. The resulting image has been smoothed by convolving a 2-arcsec standard deviation Gaussian kernel and then our optical mask of the galaxy neighbours has been overplotted. The whole process is done in order to highlight the lowest signal-to-noise features in the image. The colorbar displays the surface brightness in units of mag arcsec^{-2} . The golden ellipse shows the extent of our surface brightness analysis in the Z-band (reddest band in the optical).

Table 1. List of filters

Instrument	Filter	Exposure time [sec]	Zeropoints [mag]	PSF FWHM [arcsec]	Pixel scale [arcsec/pix]
ACS	F435W	134880	25.673	0.080	0.03
ACS	F606W	135320	26.486	0.073	0.03
ACS	F775W	347110	25.654	0.080	0.03
ACS	F850LP	346620	24.862	0.085	0.03
WFC3	F105W	333877	26.269	0.181	0.06
WFC3	F125W	193307	26.230	0.185	0.06
WFC3	F140W	82676	26.452	0.187	0.06
WFC3	F160W	317944	25.946	0.190	0.06

consistent with the limiting magnitude determinations in McLure et al. (2013).

For sampling the galaxy surface brightness profiles from our galaxy sample, we created concentric elliptical apertures from the galaxy centre, 0.5 kpc wide in the inner 2 kpc, and 2 kpc wide at greater distances. We fixed the axis ratio and position angle of these elliptical apertures to the H-band single Sérsic outputs (see Subsection 4.1), in order to sample consistently the surface brightness profiles for all filters. The H-band filter is chosen because it is the reddest and as such it

is the most representative of the total stellar component. In those annuli we estimated the galaxy flux by the 3σ clipped mean of the pixel values on those apertures, and then we apply the formula

$$\Sigma[\text{mag/arcsec}^2] = -2.5\log(F_{\text{annulus}}) + zp + 5\log(S_{\text{pix}})$$

where Σ is the galaxy's surface brightness, F_{annulus} is the average flux per pixel within the annulus, zp stands for each image zeropoint and S_{pix} is the pixel scale (0.06 arc-

Table 2. List of galaxies

Galaxy name	R.A. [J2000]	Dec. [J2000]	z_{spec}	Mass _{Chabrier} [$\log(M_{\odot})$]	Mass _{Salpeter} [$\log(M_{\odot})$]	$r_{e,H\text{-band}}$ [arcsec]	$r_{e,circ,H\text{-band}}$ [kpc]	axis ratio b/a	Pos. angle [degrees]
HUDF-1	53.16161	-27.78030	0.619	$10.42^{+0.03}_{-0.03}$	10.65	0.34 ± 0.02	1.70 ± 0.15	0.54 ± 0.01	33.44 ± 0.10
HUDF-2	53.17253	-27.78817	0.622	$10.81^{+0.16}_{-0.03}$	11.04	0.63 ± 0.06	3.06 ± 0.35	0.52 ± 0.01	-47.07 ± 0.03
HUDF-3	53.14893	-27.79976	0.664	$10.90^{+0.05}_{-0.01}$	11.13	0.42 ± 0.03	2.66 ± 0.21	0.81 ± 0.01	-26.77 ± 0.10
HUDF-4	53.16341	-27.79962	0.665	$10.81^{+0.07}_{-0.03}$	11.04	0.25 ± 0.02	1.59 ± 0.11	0.83 ± 0.01	22.04 ± 0.08
HUDF-5	53.15543	-27.79156	0.667	$11.19^{+0.09}_{-0.05}$	11.42	0.63 ± 0.05	4.16 ± 0.34	0.90 ± 0.01	75.18 ± 0.07
HUDF-6	53.15491	-27.76895	1.096	$11.43^{+0.00}_{-0.03}$	11.66	0.68 ± 0.05	4.54 ± 0.32	0.68 ± 0.01	68.52 ± 0.04

sec/pix for WFC3 and 0.03 arcsec/pix for ACS). The only object that was not totally explored using this method is HUDF-3, whose WFC3 images do not cover the whole galaxy (see Fig. 1).

4.1 Surface brightness fitting and the impact of the PSF

The Point Spread Function (PSF) of the images not only sets the angular resolution of our observations but also determines how the galaxy light is scattered (see for a recent analysis Sandin 2014, 2015). Hence, correcting the observed surface brightness profiles by the PSF distortion is essential to retrieve accurate 2D surface brightness maps and structural parameters. To that end, we have fitted using GALFIT (Peng et al. 2010), from 1 to 4 Sérsic functions to all the images of the galaxies within our sample. The reason behind our multicomponent fitting is to ensure that we are describing the 2D distribution of each galaxy’s light to the greatest level of detail permitted by our privileged photometry, avoiding any possible overmodelling ($\chi^2_{\nu} < 1$). By so doing, it is important to realize that we cannot give any physical interpretation to the different Sérsic function fits to the galaxy surface brightness profiles in ETGs, as done by other studies focused on late-type galaxies (Zibetti & Ferguson 2004; Trujillo & Bakos 2013), without the addition of kinematic information (Falcón-Barroso et al. 2006; Krajnović et al. 2008, 2013).

The Sérsic functions are axisymmetric and as such, it is impossible (unless you perform an ad-hoc fit in a particular set of pixels of your image) to model any non symmetric substructure in the galaxy’s surface brightness profiles. We thus selected as the best galaxy model the 4-Sérsic deconvolution adding the residuals of the fit –as done in Szomoru et al. (2012), hereafter “a la Szomoru” method– trying to capture any possible feature not represented by the symmetric Sérsic functions. Contrary to this “a la Szomoru” method, we masked the central 10 pixels when performing the residual addition as these central pixels have some artificial noise owing to the exact positioning of the PSF peak. Please see the Appendix A for a comparison of these “a la Szomoru” surface brightness profiles with the rest of the fits, as well as the observational galaxy profiles.

It is to note that neighbour galaxies have been masked but not subtracted in our GALFIT fits, and thus a certain level of light contamination is expected. We ensure that in all cases (except HUDF-6), none of the 5 brightest objects in each galaxy stamp is within our limit for the surface brightness determination. For our exception, HUDF-6 images show

a companion star at ~ 10 arcsec from the galaxy’s centre. The difference between fitting or not (using of course a PSF model) this star for the galaxy total flux is $< 0.02\%$, and thus negligible.

Our PSF choice must not only be accurate but very extended as well, in order to prevent any red spurious excess at large radii mimicking the light contribution of a stellar halo (the so-called “red halo” problem, e.g. Zibetti et al. 2004; Zibetti & Ferguson 2004; Zackrisson et al. 2006; de Jong 2008). In theory, we should go as far as 1.5 times the full galaxy size (Sandin 2014, 2015; Trujillo & Fliri 2016). Tiny Tim (Krist 1995) is the only way to build such extended HST PSFs. Therefore, we created our Tiny Tim simulated stars by assuming they should extend up to the equivalent size of 200×200 kpc at the median redshift ($\langle z \rangle = 0.65$) of our galaxy sample. This translates into PSF sizes of 500×500 pixels for WFC3 and 1000×1000 pixels for ACS. However, for ACS images, Tiny Tim cannot retrieve models spanning such large distances, and thus we content ourselves with the maximum extent possible for this camera. However, this fact has very little (if any) impact in our analysis because of the very small sizes of our passive galaxy sample in the bluest bands.

We further improved the PSF produced by Tiny Tim in each band by replacing the core with that of an isolated non-saturated star at RA=03:32:38.01, DEC=−27:47:41.67 (J2000). This mitigates the effect shown by Bruce et al. (2012) whereby Tiny Tim underpredicts the PSF flux at distances greater than 0.5 arcsec. We also rotated these hybrid stars in order to match the position of the stellar spikes in HUDF science image. The chosen stars spectral type is K4-K5 star (Pirzkal et al. 2005), which is optimal for studying early-type galaxies as the light from both the star and the galaxies is scattered similarly in broadband filters (La Barbera et al. 2012).

After these considerations on our PSF model, we checked about the existence of the “red halo” problem in our sample. The test we performed is to be found in Figure 4. We compare there our observed surface brightness profiles, the “a la Szomoru” profiles and the PSF profiles (scaling them up to match the peak in the galaxies’ surface brightness profiles). These are space observations (small PSF FWHM), and as such there is not so much difference between the convolved and unconvolved + residuals profiles. It is also reassuring that the outer parts of the galaxies do not decrease in a similar way as the PSF profiles, and thus limiting the impact of the “red halo” problem. What we find is that there is an exponential decay for HUDF-2 in the NIR bands between 3 and 8 arcsec, indicating the presence of an

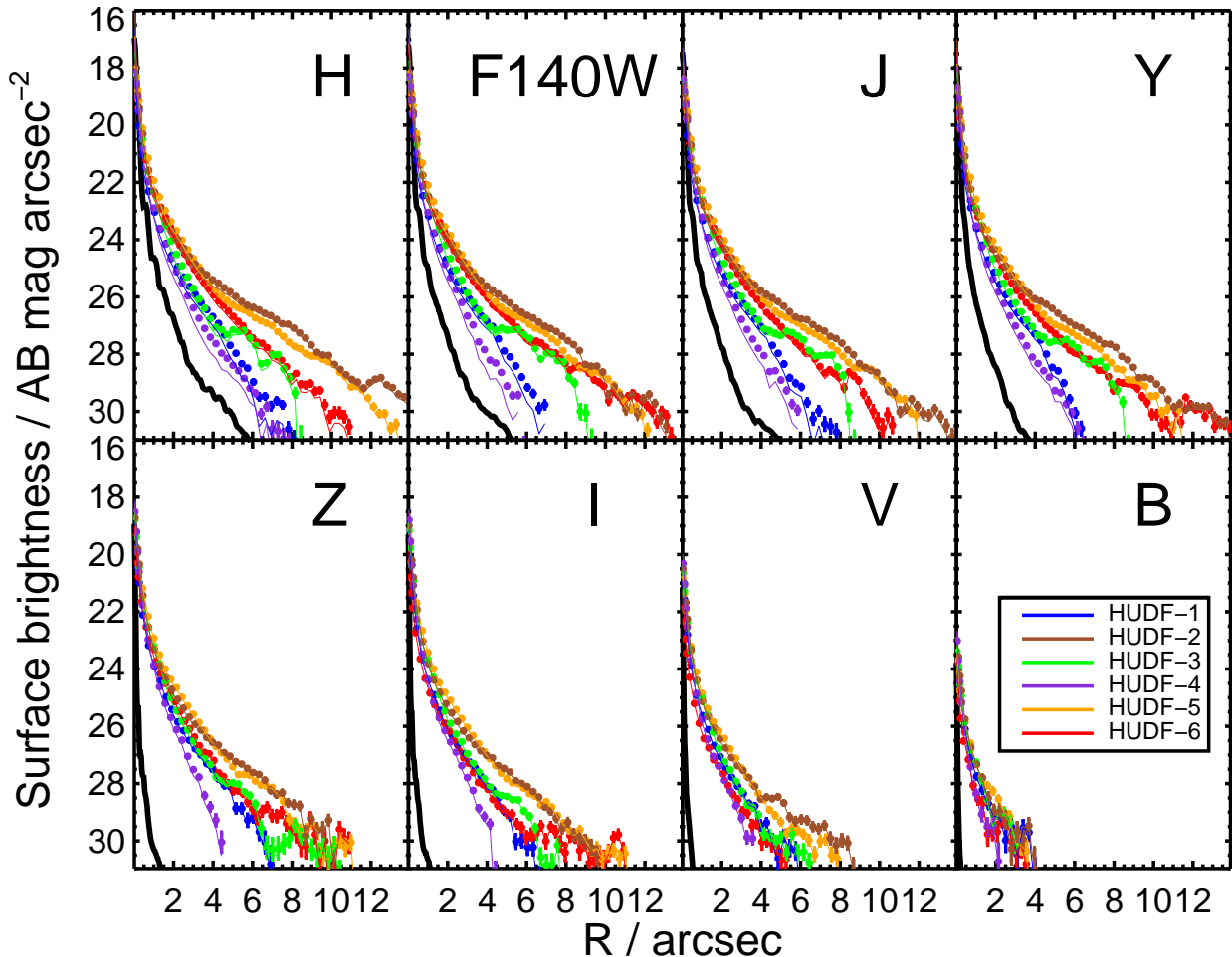


Figure 4. Comparison among the observed galaxy surface brightness profiles (coloured points), the best galaxy surface brightness models (“a la Szomoru”: deconvolved profiles + residuals; coloured lines) and the PSF profiles (scaled up to match the galaxy centres; black lines) for each HST band. As expected for large early-type galaxies in space observations (small PSF FWHM) the convolved and unconvolved profiles are not very different. Moreover, the outer parts of the galaxies do not decrease their brightness in a similar way than the PSF profiles, limiting any “red halo” issue in our sample.

inner disk. We will further discuss about it in Section 5.4. Finally, we did another similar exercise comparing star and galaxy profiles, but normalizing this time the PSFs to the total galaxy fluxes. We obtained similar conclusions.

5 RESULTS

We show our observed surface brightness profiles in Figure 5. It is worth noting that the various galaxies in our sample show emission extending to different galactocentric distances and that none of them have signs of abrupt truncation even at the faint levels explored. Every galaxy is more extended and more luminous in the redder bands as expected for passive ETGs. For some of the objects, we reach 10-12 arcsec in the H-band, which is comparable to local Universe very deep observations (Kormendy et al. 2009;

Tal & van Dokkum 2011) but this time at a median redshift $z \approx 0.65$ where the cosmological dimming makes all galactic features ~ 2 mag arcsec $^{-2}$ fainter.

5.1 Sloan equivalent filters and colours

We have calculated Sloan bands equivalent restframe surface brightness profiles for the six galaxies in our sample (Fig. 6) for determining colours and masses at each step in galactocentric distance. They were constructed from both the observed and the model+residual “a la Szomoru” profiles by linearly interpolating the HST filters and then correcting the surface brightness by cosmological dimming (as done before in Trujillo & Bakos 2013). It is noticeable that the PSF effects are more pronounced for the central parts where the galaxy flux is more concentrated, and for the redder filters, as the WFC3 PSF is broader than the ACS one. As

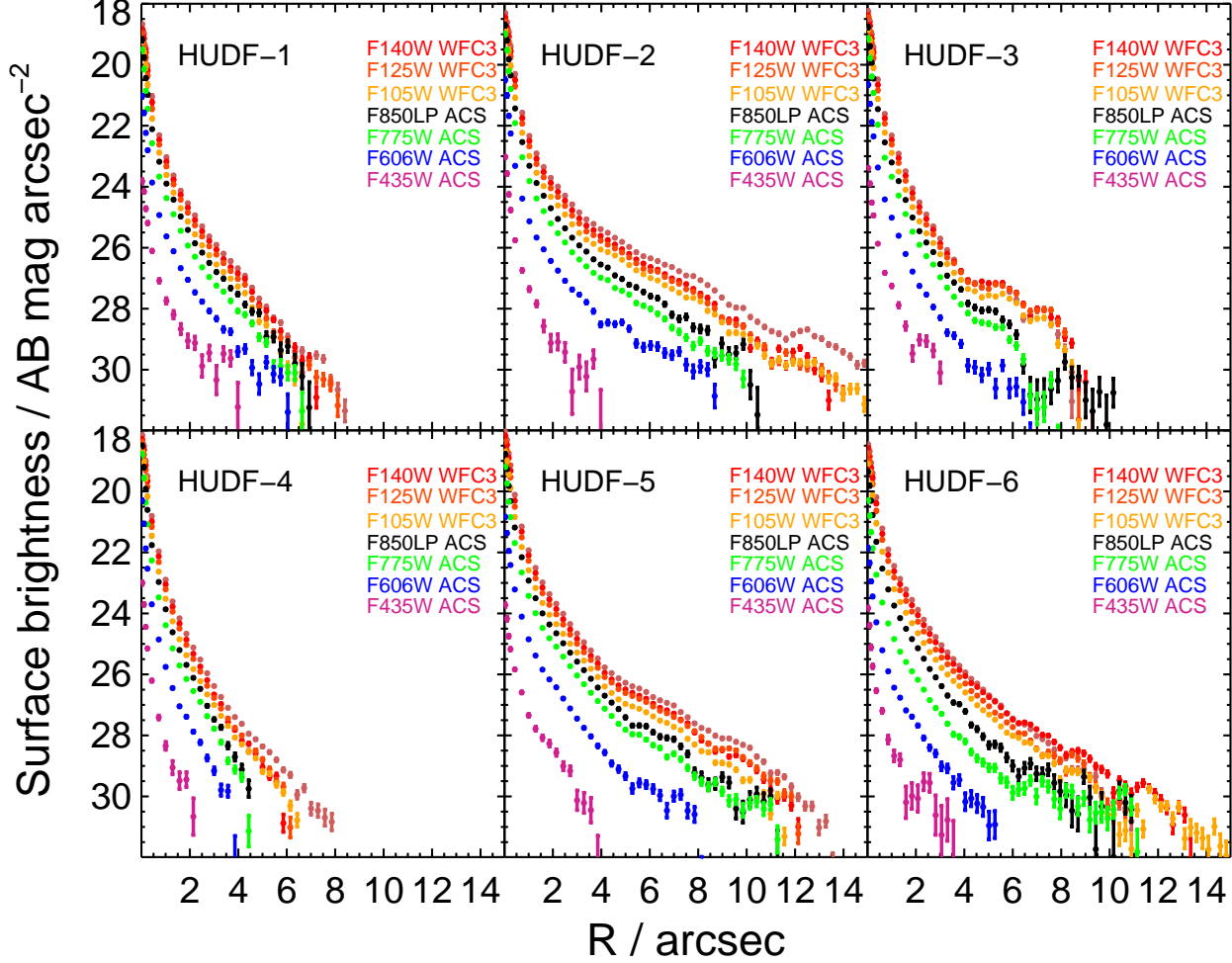


Figure 5. Observed surface brightness profiles measured within each of the HST filters available for our ETG sample. Each individual point was calculated in elliptical 2 kpc wide apertures (except for the central four points where 0.5 kpc wide apertures were used), applying a 3σ clipped mean in those annuli, for retrieving the surface brightness values and the associated error bars. For all cases, these massive ETGs are more luminous and extended in the redder bands. The galactocentric distances probed in this study, sometimes more than 100 kpc at $z = 0.6 - 1$, are comparable with local Universe ETG very deep observations (Kormendy et al. 2009; Tal & van Dokkum 2011).

expected, correcting for the PSF produces brighter galaxy cores and slightly fainter profiles at intermediate galactocentric distances, while at larger distances (> 30 kpc) the effect is almost negligible. For the galaxies HUDF-2, HUDF-3 and HUDF-5, a number of quite distinctive surface brightness bumps at magnitude ~ 25 are visible. They are especially strong for the redder bands. In the latter two cases, the association with recent merger events is evident, looking at the visual morphologies in the NIR bands. For the remaining one, this may be also the case, as it looks very asymmetric in the same photometric bands.

With these profiles, we computed the Sloan filters equivalent $u - g$, $u - r$, $g - r$, $g - z$ and $r - i$ colours in Figure 7 up to 30 kpc. The inner parts of the colour profiles are uncertain due to the few pixels that enter in our concentric ellipses for the surface brightness calculations. For instance,

observing with WFC3 (0.06 arcsec/pix) a galaxy at $z = 0.65$ (~ 7 pix/arcsec) means that the inner kpc is comprised in a radius of ~ 2 pixels. After the central kpc, the profiles are rather flat. We choose not to show beyond 30 kpc because of the larger error bars (> 0.2 mag) and also upbends in some profiles. The reason behind these odd colours at large galactocentric distances is the aggressive sky subtraction, as the HUDF was optimized to look for high- z galaxies, and therefore any very extended structure is affected even with our careful data reduction.

5.2 Stellar mass profiles

Figure 8 shows the circularized stellar mass density profiles for the galaxies in our sample. We calculated them using the prescriptions in Roediger & Courteau (2015) Appendix

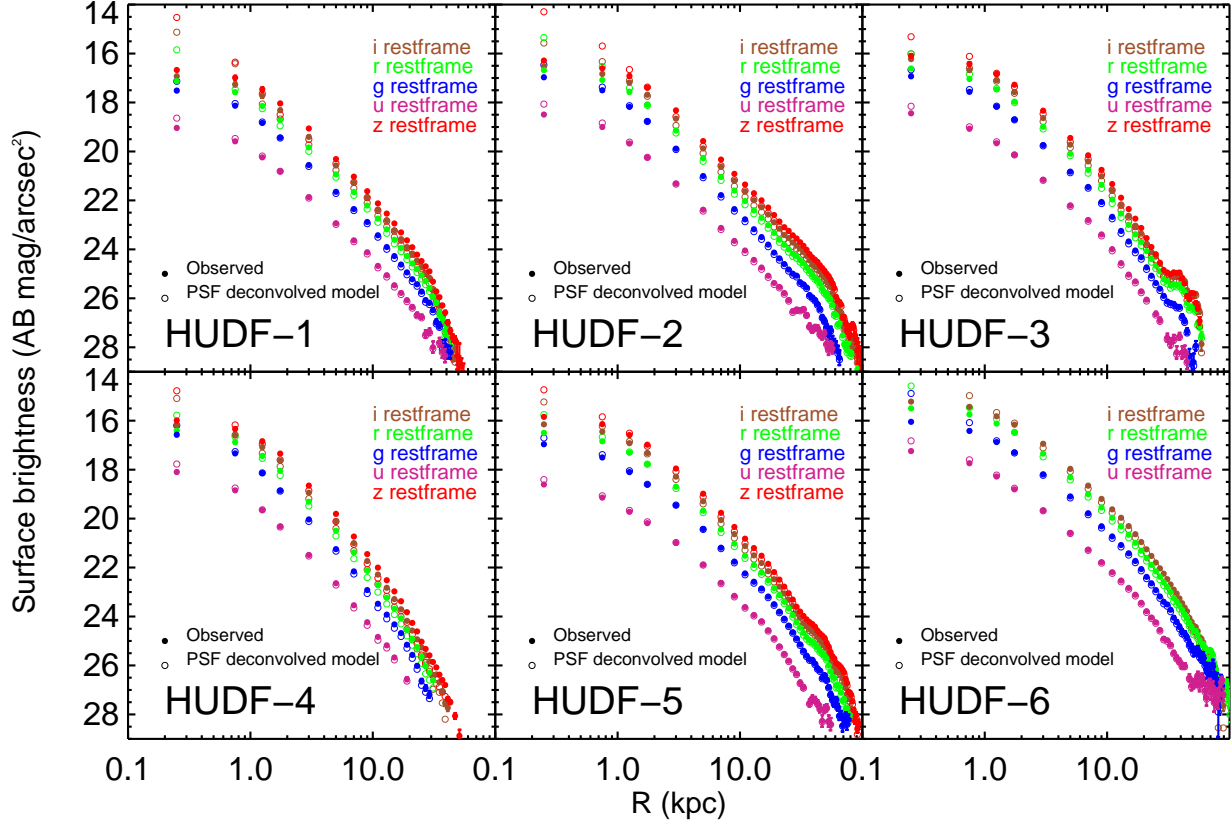


Figure 6. The u , g , r , i and z -band Sloan filters equivalent restframe surface brightness profiles for the six galaxies in our sample. They were created by linearly interpolating the HST filters, both for the observed and the model+residual “a la Szomoru” profiles, and then correcting the surface brightness by cosmological dimming. Note that, for HUDF-6, z -band is not covered due to its redshift ($z \sim 1.1$). It is clear that the PSF effect scattering the light coming from these objects is more pronounced for the inner galaxy parts. It is also interesting checking that HUDF-2, HUDF-3 and HUDF-5 have bumps at restframe surface brightness 25-26 mag arcsec $^{-2}$, and they are specially strong in the redder bands. By joining this information with their visual appearance, we associate these features to recent merging events.

A Table 2 for mass-to-light ratios using Sloan colours. Specifically, for the galaxies at $\langle z \rangle = 0.65$, our choice of colour and base profile was $g-z$ and z , and for HUDF-6 we utilized $u-r$ and r . These sets of colours and bands were chosen in order that the blue band is only constructed from the ACS filters and the red band uses only WFC3 information. Consequently, we avoid any PSF mismatching effects that may arise in case one combines photometric data coming from two different cameras. We normalized the total masses by those obtained from the SED fitting. Overplotted are the mass profiles for similar mass ($8 \times 10^{10} < M_{\text{stellar}} / M_{\odot} < 1.2 \times 10^{11}$) ETG galaxies (Sérsic index $n > 2.5$) in NYU catalog (Blanton et al. 2005) at $0.08 < z < 0.12$ (the uncertainties are given as a shaded red region) and the massive and compact galaxies in Szomoru et al. (2012) at 1.75

$< z < 2.5$ (with mean $r_{\text{e,circ}} = 0.98$ kpc and $n = 3.92$). For both our sample and Szomoru et al.’s, we provide the individual and mean profiles. We choose to stop ours at 30 kpc in order not to be affected by any colour uncertainties in our light-to-mass conversions. Our sample of massive HUDF ETGs show extended stellar haloes not present in the compact high- z galaxies (Bezanson et al. 2009; Cassata et al. 2010; Szomoru et al. 2012; Trujillo et al. 2014), thus showing closer resemblance to the SDSS local counterparts.

In order to parametrize this variation, we have integrated these mass mean profiles between 10 and 50 kpc, where we can compare our results with state-of-the-art simulations (Cooper et al. 2013, see Section 5.3 in the present paper). As neither Szomoru’s nor our mass profiles extent to that distance, we fit the mean profiles in the two cases

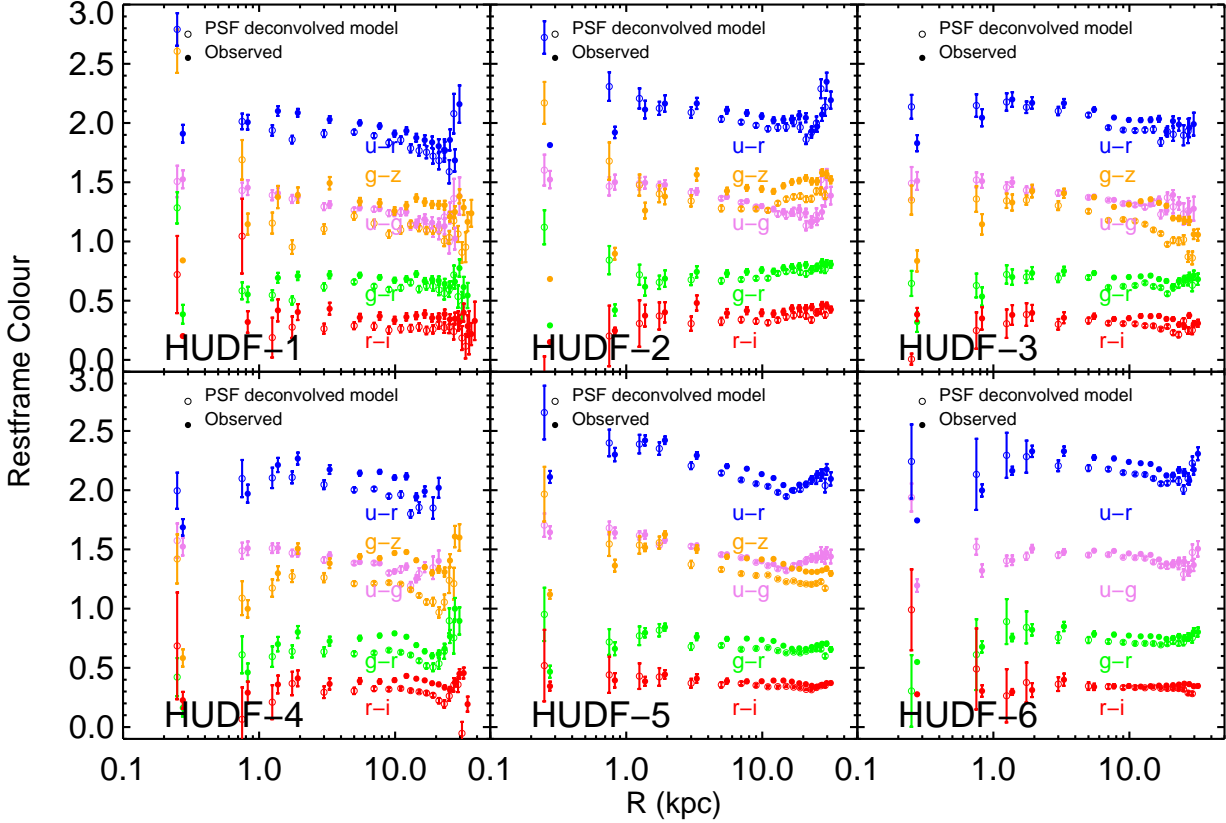


Figure 7. The $u - g$, $u - r$, $g - r$, $g - z$ and $r - i$ Sloan filters equivalent restframe colour profiles for the six galaxies in our sample. Both observational and model+residual “a la Szomoru” profiles are plotted (with a slight shift in the x-axis for a better reading), along with their errors up to the limit of 30 kpc.

to Sérsic functions and extrapolate these functions up to 50 kpc. Then we integrate these functions between 10 and 50 kpc. The results are remarkable: while 3.5% of the galaxy mass is enclosed at these distances for Szomoru et al.’s case ($\langle z \rangle = 2$), the fraction is 15.1% at $\langle z \rangle = 0.65$ and 28.7% at $\langle z \rangle = 0.1$. Despite the fact that the total stellar mass for the three mean profiles is similar ($\sim 10^{11} M_{\odot}$), the mass profiles of massive ETGs at high- z are intrinsically different than those at lower redshifts.

In figure 9 we provide a more in-depth quantification of the amount of light (both for the reddest filter, the H-band, and the z-band restframe which is the band we used to build the mass profiles) contained in the galaxies of our sample using the same elliptical apertures we utilized for deriving the surface brightness profiles. Between 20% and 40% of the light is distributed at distances beyond 10 kpc. The only massive galaxy that differs slightly (more light concentrated in the inner parts and less in the outskirts) is the compact HUDF-4. It is not possible to discern any sharp transition

between the galaxies’ cores and their external parts by either visually inspecting these plots or the mass profiles in Fig. 8.

5.3 Comparison with state-of-the-art simulations

In this subsection we compare our observational results with the theoretical models of Cooper et al. (2013, hereafter C13). These simulations use a semi-analytic model of galaxy formation (Guo et al. 2011) in combination with a cosmological N-body simulation (Boylan-Kolchin et al. 2009) to predict the surface mass density profiles of ~ 1900 galaxies hosted by dark matter haloes of mass 10^{12} - $10^{14} M_{\odot}$.

In simulations it is possible to distinguish stars that are accreted by galaxies from so-called in-situ stars formed directly in their host dark matter haloes. In observations, the various subcomponents of late-type galaxies follow different light distributions, allowing the canonical bulge-disk-halo decomposition (e.g. Trujillo & Bakos 2013). In ETGs, however, both in situ and accreted stars are distributed in

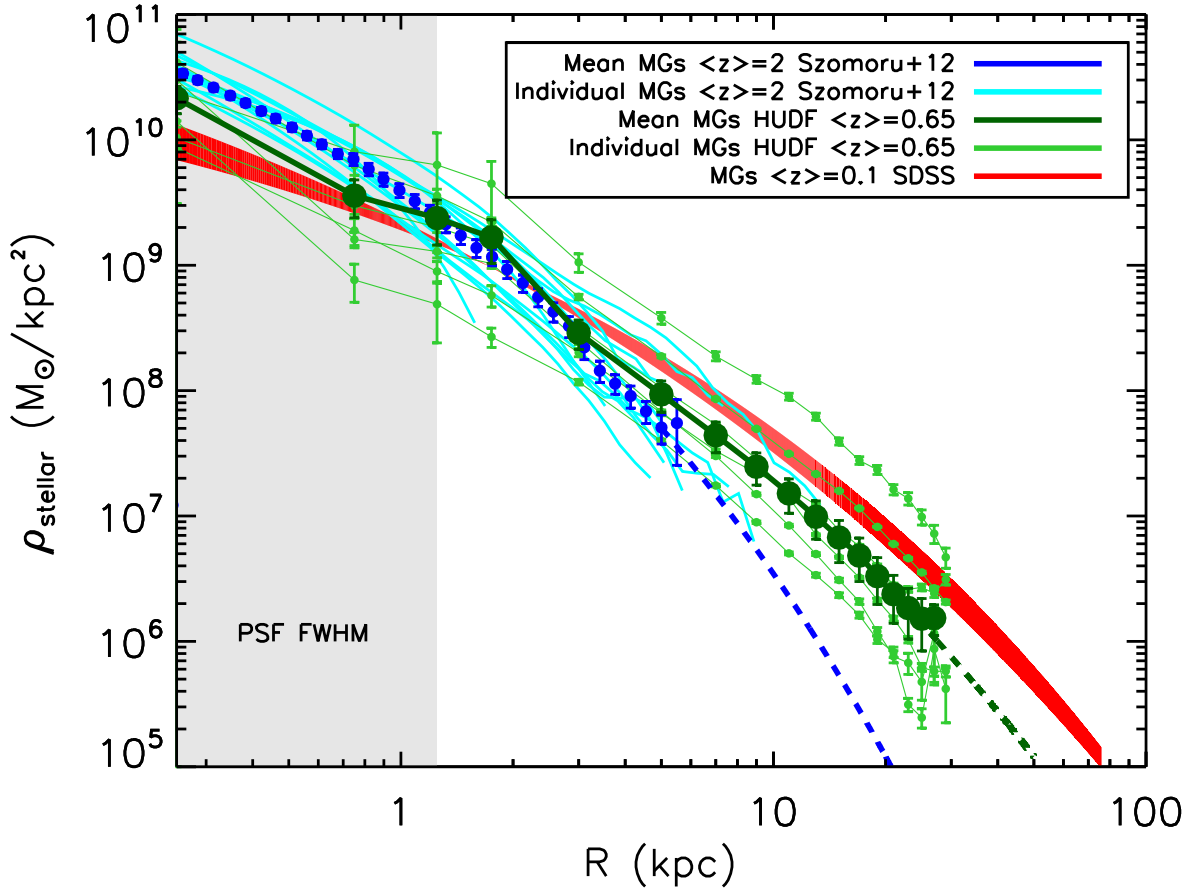


Figure 8. The circularized stellar mass density profiles for the Massive Galaxies (MGs) in our sample, comparing them with similar mass SDSS ETGs and the massive compact galaxies in Szomoru et al. (2012). Individual mass profiles are shown in light colours, while the mean profiles are in dark colours (and their extrapolations are the dashed lines). HUDF massive galaxies show an excess of mass in their outer parts, opposite to what could be seen for the high- z sample, and closer what was found for local massive ETGs. This evidence points to the progressive building up of stellar haloes as the link between the two other populations.

spheroidal components that cannot be separated unambiguously by decomposition of their surface brightness profiles. To proceed, we make use of the fact that the C13 models predict that accreted stars have much lower binding energies on average than in situ stars, with the result that essentially all stellar mass beyond a certain galactocentric radius is accreted. The mass obtained by integrating both observed and simulated mass profiles outwards from a sufficiently large radius therefore provides a fair point of comparison, even though it does not correspond to the total mass of accreted stars in either case.

In the C13 simulations, late and early types are separated by the ratio of bulge to total mass predicted by the Guo et al. (2011) model (B/T less or greater than 0.9 respectively). The particle tagging method used by C13 to predict surface brightness profiles introduces an additional free parameter beyond those of the Guo et al. model, f_{mb} . This controls the depth in the host dark matter potential at which newly-formed ‘stars’ are inserted into the simulation. For example, a value of $f_{mb}=1\%$ means that newly

formed stellar populations initially have a binding energy distribution identical to that of the most tightly-bound 1% of the dark matter in their host dark matter halo (see C13 for details). C13 explore a range of values for this parameter, which they find to be strongly constrained to a range 1-5% by the observed size-mass relation of galaxies dominated by in situ stars (i.e. discs) at $z=0$. In practice, the precise choice of f_{mb} makes only a very marginal difference to the results we discuss here (Cooper et al. 2013; Trujillo & Fliri 2016). We therefore report comparisons against the $f_{mb} = 1\%$ results of C13.

The further from the centre of the galaxy, the lower is the contribution by in situ material to the mass profile. Being conservative, we will start our integration from the typical distance where high- z massive galaxy surface brightness profiles finish (~ 10 kpc, see Fig. 8) and hence identify our stellar haloes as the light component previously missed in shallower observations. We stop our calculations at 50 kpc, our previous integration limit. The results for our galaxy sample are plotted in Figure 10, and their error bars

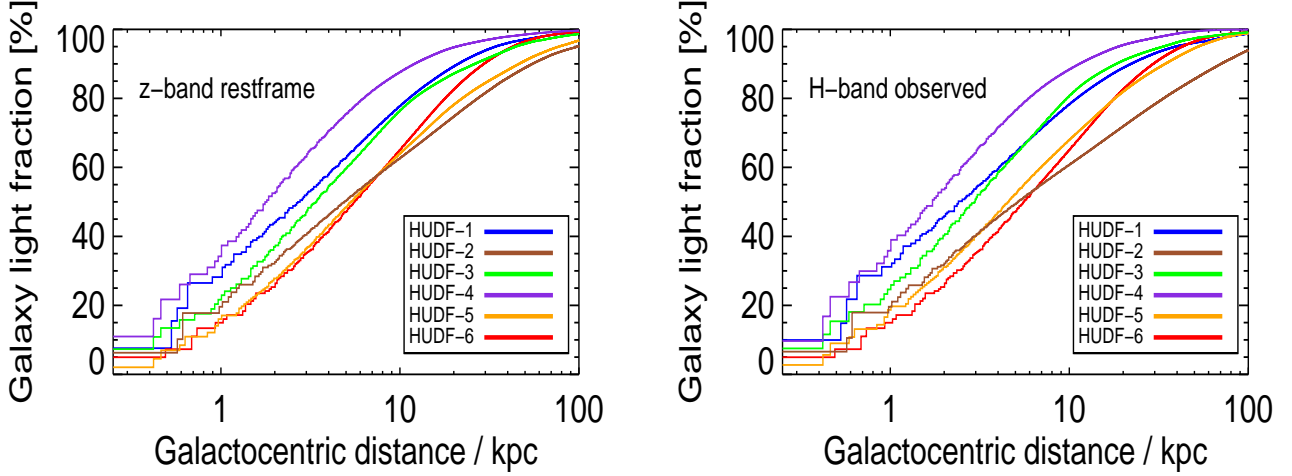


Figure 9. Cumulative light fractions for our inferred z-band restframe (the base for our mass profiles) and the reddest observed band (H). Except for HUDF-4, the most compact galaxy, the rest of the massive galaxies store between 20 and 40% of their light at galactocentric distances greater than 10 kpc.

stem from the difference in the mass determinations by using either the Roediger & Courteau (2015) or the Bell et al. (2003) recipes. We also supply the local galaxy mass fraction at $10 < R / \text{kpc} < 50$ relationships from the Cooper et al. (2013) simulations for ETGs. This relationship is displayed in red colour, with the 16 and 84 quartiles being the dashed lines. For consistency, we also overplot the extrapolations for the individual massive ETGs in Szomoru et al. (2012) and the mean values for the three samples we are using throughout this paper (namely Szomoru’s, HUDF and SDSS).

There is an overall departure of our galaxy sample from the local relation, most probably due to the fact that they are not $z = 0$ galaxies ($\langle z \rangle = 0.65$ median redshift). In fact, the six massive galaxies in our sample straddle the high- z and low- z data. Combining the location of the $\langle z \rangle = 2$ data points and Fig. 8, it seems that the HUDF ETGs are advancing towards the upper part of the plot to reach their fiducial $z = 0$ relation. Very interestingly, there is a correlation between the total galaxy mass and fraction of mass in the outer parts for our six galaxies, where they approximately follow the Cooper et al.’s ETG predictions. It is also remarkable the agreement between Cooper’s simulations and the SDSS mean value.

Quantitatively, Figure 8 (left side) in Trujillo & Bakos (2013), Figure 4 in van Dokkum et al. (2014) and Figure 13 in Trujillo & Fliri (2016) show that the haloes of $M_{\text{stellar}} \sim 10^{10} - 10^{11} M_{\odot}$ late-type galaxies constitute at most 5% of their total light at $z = 0$. Our small but unique sample shows that the stellar mass in massive ETG stellar haloes is larger, of the order of 5-20% (and yet not at $z = 0$, but at $z \sim 0.65$). This contrast between galaxy types must be investigated further (see for instance D’Souza et al. 2014), but makes sense from a Λ CDM perspective, where the histories of ETGs should be more merger-dominated than for disk galaxies (Cole et al. 2000; Croton et al. 2006; Purcell et al. 2007; Ruiz et al. 2015), and also because ETGs do not have

a prominent disk storing a significant fraction of the galaxy’s baryons.

5.4 Constraining the merger channel for massive galaxy growth

Studies about merger rates always provide an indirect way to look at the assembly history of galaxies, because of the fact that what it is measured is the mass to be accreted as opposed to accreted mass. It is interesting to see whether this could be improved by using very deep images to trace any signature of ongoing merging.

To this end, we have created the following exercise. We take the galaxy light which is not described by the overall galaxy spheroid, i.e., the residuals from subtracting the single Sérsic fit to each galaxy surface brightness profile. Converting those into mass (in an approximate manner, given the information at hand) we can check their relative importance. The reason behind this exercise resides in the fact that some low surface brightness features come from galaxy interactions (at least in HUDF-2, HUDF-3 and HUDF-5). These features are smooth and, as such, very hard to be picked up as potential close pairs. HUDF12 has the potential to detect them at intermediate redshift, opening a new perspective in the mass assembly of massive galaxies.

Nevertheless, we would like to emphasize that this is just a toy model because of fitting a single Sérsic function to deep and high resolution images of most ETGs, even in the local universe, leaves residuals which have nothing to do with merging features. This seems to be the case for HUDF-1 and HUDF-2, as their residual images display negative and positive values close to the galaxy centre in perpendicular directions corresponding to the symmetry axes, typical of the presence of a non-subtracted inner galaxy disk (as detected in Section 4.1). Therefore, for these two galaxies, we investigated the residuals coming from the subtraction of a double Sérsic fit instead of a single Sérsic fit.

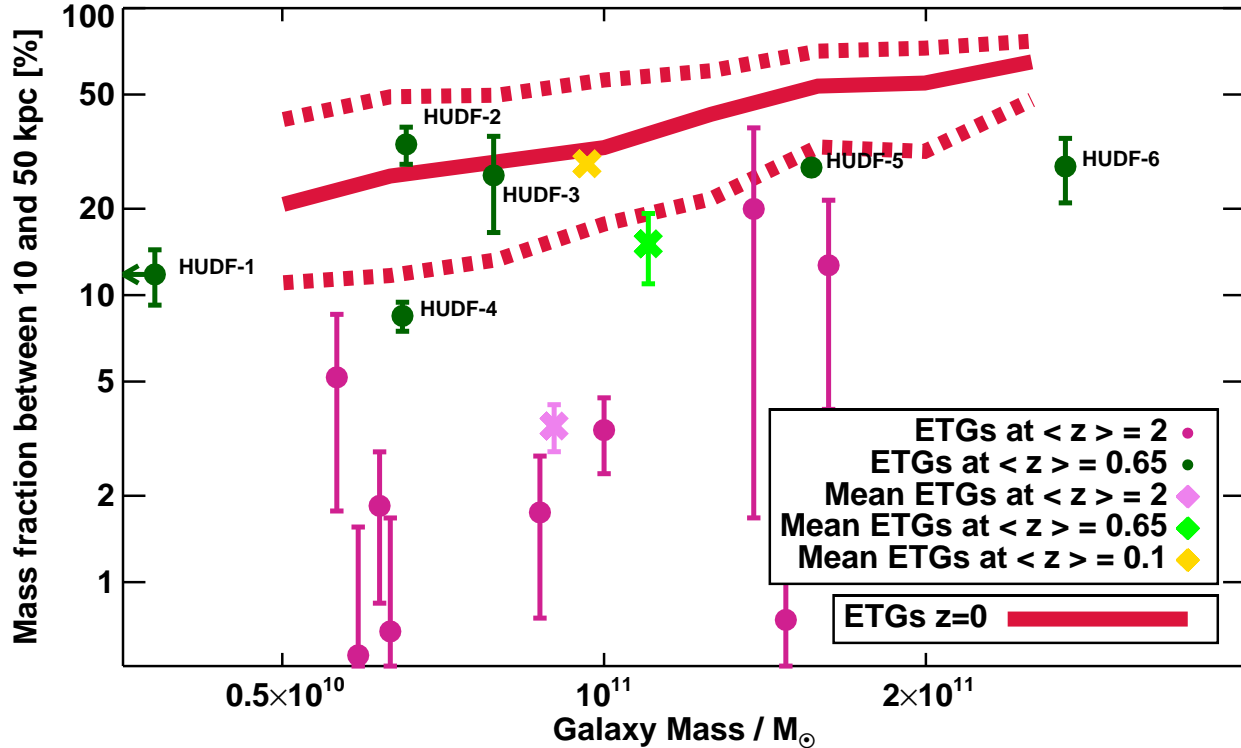


Figure 10. Fraction of the galaxy stellar mass between 10 and 50 kpc versus the total stellar mass for our sample of six Early-Type Galaxies (ETGs; the green points). Our inferred mass fractions come from the recipes in Roediger & Courteau (2015), and the errors from the absolute differences between those and the ones in Bell et al. (2003) (HUDF-5’s errors are too small to be seen). The solid red lines are the results for local ETGs in Cooper et al. (2013) simulations, with the dashed lines corresponding to the 16-84 percentile range. The violet data points are individual massive galaxies at $\langle z \rangle = 2$ studied in Szomoru et al. (2012), but we want to emphasize that they are extrapolations as information about their mass profiles is unavailable at these galactocentric distances. The crosses in light violet, light green and golden colours denote the mean values for the $\langle z \rangle = 2$, $\langle z \rangle = 0.65$ and $\langle z \rangle = 0.1$ massive galaxy samples respectively (cf. Fig. 8). There is a rough correlation between galaxy mass and the percentage of mass in the outskirts for the green points, following the simulation predictions. However, it is to note that our data do not follow the local relationship because of the median redshift of our sample ($\langle z \rangle = 0.65$). Most importantly, 5-20% of ETGs stellar mass is located in their “haloes”, above the high- z data points and in stark contrast with recent results for late-type galaxies (Trujillo & Bakos 2013; van Dokkum et al. 2014; Trujillo & Fliri 2016).

The step to transform from light to mass is done by a crude assumption, i.e. that the mass to light ratio is constant through the entire radial distribution. Considering that our galaxy sample have relatively flat colour gradients, this is reasonable. We utilize the value given by the MIUSCAT models⁴ (Vazdekis et al. 2012; Ricciardelli et al. 2012) in the reddest (SDSS i-band) mass-to-light ratio provided assuming Kroupa universal IMF, solar metallicity and a stellar population age of 5 Gyr. The results are given in Table 3 and Figure 11. The errors stem from the different total amount of light enclosed in the HST residuals closest to restframe i-band.

Very little light is involved in these smooth features (of the order of 1% the galaxy light), with a slightly larger percentage in mass (1-2%). To put these numbers in context, we compare them with best estimates from satellites/close

pairs. Specifically, Ferreras et al. (2014) with a sample of 238 massive galaxies at $0.3 < z < 1.3$ quantified that the upper limit for the average mass growth rate for these galaxies is $(\Delta M/M)/\Delta t \sim 0.08 \pm 0.02 \text{ Gyr}^{-1}$, while van Dokkum (2005) inferred $0.09 \pm 0.04 \text{ Gyr}^{-1}$ for 126 red nearby galaxies. To move from growth rate to mass, a timescale for the duration of the morphological features of dry mergers should be adopted. Bell et al. (2006) classified major (1:1 to 3:1) merger snapshots suggesting values of $150 \pm 50 \text{ Myr}$. The duration of the visibility of galaxy mergers using CAS parameters is 0.4-1 Gyr (Conselice 2006; Lotz et al. 2008; Conselice et al. 2009). Choosing then 0.5 Gyr as a representative number, one would expect $\sim 4\%$ of the total mass of the galaxy in these residuals.

Our numbers are close to these expected values, especially by thinking that some residuals in mass are not seen because of our masking. Actually, this aspect makes our measurements a lower bound in the percentages of light and

⁴ <http://www.iac.es/proyecto/miles/>

mass. Nevertheless, we believe we cannot draw any strong implications as this experiment has many parameters we do not control: the residuals and the mass-to-light ratios being representative of substructures, the uncertainty about how long merging features last and cosmic variance due to the fact of studying only six massive galaxies. It is to note that the galaxies showing smaller residuals are two most compact ones (HUDF-1 and HUDF-4) and the most distant galaxy (HUDF-6) which might be an indication that cosmological dimming has a deeper impact on it than for the rest of the objects, hiding some extra mass in undetected features. Summarizing, it is very interesting to see that this naive exercise yields numbers similar to close pairs predictions and also to check that the visually identified merging smooth features in HUDF-2, HUDF-3 and HUDF-5 clearly provide to these galaxies with more mass in their residuals.

6 SUMMARY AND CONCLUSIONS

We present a comprehensive characterisation of the six most massive ($M_{\text{stellar}} \geq 5 \times 10^{10} M_{\odot}$) Early-Type Galaxies (ETGs) at $z \lesssim 1$ in the deepest HST field, the HUDF. We focused our efforts in the HUDF12 programme (Ellis et al. 2013; Koekemoer et al. 2013), whose data reduction preserves extended low surface brightness features and at redshifts where cosmological dimming is not yet strong enough ($\lesssim 2 \text{ mag arcsec}^{-2}$) to remove the traces of minor merging.

The substructures present in the outer parts of ETGs, whose origin is the progressive build-up of these objects via merging, have not been studied to date at intermediate/high redshift due to their intrinsic faintness and the very rapidly growing cosmological dimming, which make these outskirts very challenging to detect. Therefore, it is not yet known whether these outer parts could be described as galactic haloes, similar to those found in disk galaxies. Our work aims to clarify this situation and investigate how massive galaxies change their observational properties since $z = 1$.

We carefully analysed each galaxy image according to the recipes in Trujillo & Bakos (2013), fitting up to 4 Sérsic functions convolved with the PSF in the 8 HST filters available. In so doing, we are able to remove the PSF distortion in the observed profiles. Our ultra-deep dataset reaches galaxy surface brightness profiles down to $31 \text{ mag arcsec}^{-2}$ (3σ in $10 \times 10 \text{ arcsec}$ boxes; $\sim 29 \text{ mag arcsec}^{-2}$ after correcting by cosmological dimming), which translates into 25 effective radii in distance, or as far as 100 kpc in some cases at an outstanding median redshift of $\langle z \rangle = 0.65$.

The striking difference between previous shallower observations and the HUDF12 is the appearance of extended low surface brightness envelopes (or stellar haloes) for each individual galaxy. Even though the small statistical representativeness of our sample, containing only 6 objects, our dataset is unique inasmuch as we demonstrate the existence, the relative importance and the spatial distribution of this low surface brightness component for each individual galaxy at study. Of course, longer integration times disclose fainter and fainter features (e.g. Martínez-Delgado et al. 2010; Duc et al. 2015; Trujillo & Fliri 2016), which are key to understanding the assembly history of massive galaxies,

although their contribution to the total light and mass decrease in importance. We stress that caution needs to be taken with image data reduction, as indeed the images must be reduced in such a way to preserve low surface brightness features. Providing we work in this direction, the advent of very deep imaging in future years will not only improve our understanding of high redshift galaxies but will also greatly enhance our comprehension of the nearby Universe.

We placed constraints on the inside-out growth of massive ETGs by estimating their observed surface brightness profiles, equivalent Sloan filters restframe profiles and colours, mass profiles and light cumulative fractions. Both HST bands and the Sloan filters equivalent photometry show a steady decrease in galaxy flux down to our detection limit without the presence of any truncations. Galaxies displaying signs of merging have surface brightness bumps in their outer parts (at $> 20 \text{ kpc}$; $25\text{--}26 \text{ mag arcsec}^{-2}$ restframe). In general, between 20% and 40% of the light is located at distances beyond 10 kpc. Additionally, when comparing the mean massive ETG mass profiles at different cosmic times, we find that they store a higher fraction of stellar mass in their outer parts (same galactocentric distances) at decreasing redshift, namely 28.7% at $\langle z \rangle = 0.1$, 15.1% at $\langle z \rangle = 0.65$ and only 3.5% at $\langle z \rangle = 2$.

It is very hard to unambiguously define ETG stellar haloes (especially without kinematic information), or even comparing with in-situ/accreted material in numerical simulations. However, by integrating both the observational and simulated mass profiles at distances ($10 < R/\text{kpc} < 50$) where hierarchical accretion is dominant over the in-situ formed stars, we gather evidence for ETG haloes containing more mass than their late-type counterparts. ETG galaxy stellar haloes host 5-20% of the galaxy mass, in stark contrast with what has been reported for late-type stellar haloes (see Fig. 12 in Trujillo & Fliri 2016, only up to 5%). We must emphasize that the median redshift of the six galaxies at study is $\langle z \rangle = 0.65$, and hence this divergence between early- and late-types is larger for local Universe massive ETGs. Extended low brightness components are present in all massive ETGs in our sample and they seem to be a ubiquitous ingredient of the Λ CDM paradigm.

Finally, we developed a toy model in order to attempt to determine the total amount of light and mass in smooth features linked with ongoing minor merging interactions. Our parametric fits allow us to model the overall spheroid in each galaxy of our ETG sample. After removing this 2D surface brightness profile, the residual light gives us insight into the ongoing mass assembly as opposed to more indirect methods such as satellite counts. The uncertainties are large, due to the necessary assumptions and the inherent scatter in a galaxy-by-galaxy basis, but the results of this experiment indicate that smooth merging features in our imaging contribute at least 1-2% in galaxy light and mass. The expectation from close pairs is $\Delta M/M \sim 4\%$, and our result must be further investigated, but it does not contradict the fact major and minor mergers seem to be the dominant mechanisms driving the evolution of massive ETGs since $z = 1$.

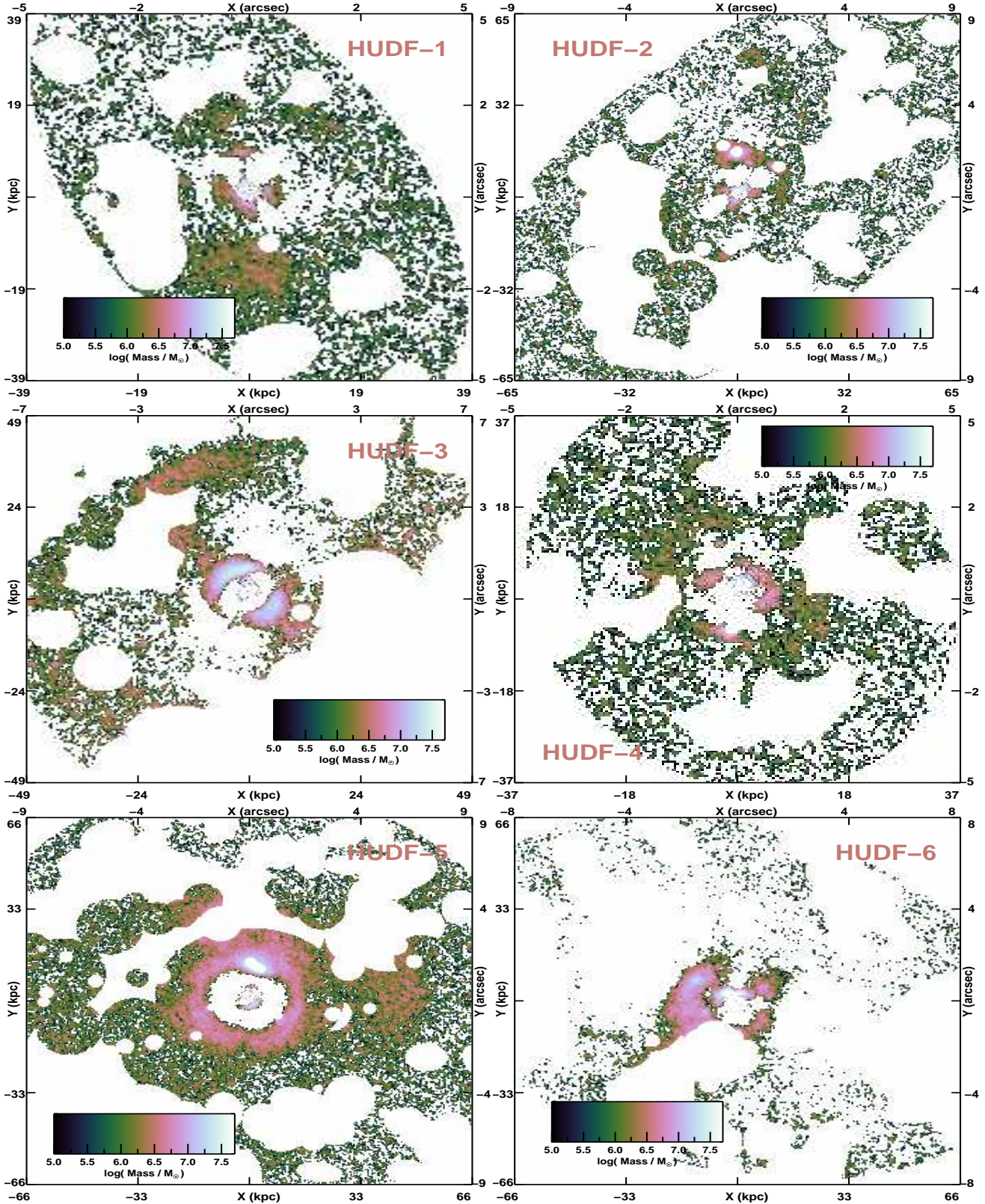


Figure 11. Stellar mass maps corresponding to the smooth residuals in the galaxy light. Thinking of the inside-out growth of massive galaxies, we calculated how much mass is encompassed in minor interactions by subtracting to every galaxy a Sérsic model of its overall spheroid. The colour coding is the same throughout the plots, but each galaxy is shown up to its full extent ($31 \text{ mag arcsec}^{-2}$). The white elliptical patches are the product of neighbour masking, and thus the total masses listed in Table 3 for these residuals (1-2% of the total galaxy stellar mass) should be taken as a lower limit. These numbers given by our toy model are not far from the predictions from close pairs to the mass growth of massive ETGs ($\Delta M/M \sim 4\% \text{ Gyr}^{-1}$).

Table 3. Stellar mass contained in the residuals

Galaxy	% light in residuals i-band	Mass $\times 10^8 M_\odot$	% galaxy's mass
HUDF-1	0.52 ± 0.06	2.06 ± 0.24	0.79 ± 0.09
HUDF-2	1.03 ± 0.07	10.24 ± 0.71	1.57 ± 0.11
HUDF-3	1.79 ± 0.47	21.47 ± 5.64	2.72 ± 0.71
HUDF-4	0.35 ± 0.10	3.49 ± 0.97	0.54 ± 0.15
HUDF-5	1.41 ± 0.01	33.53 ± 0.31	2.15 ± 0.02
HUDF-6	0.34 ± 0.13	14.15 ± 5.38	0.52 ± 0.20
<i>Mean values</i>	0.91 ± 0.13	14.16 ± 1.69	1.38 ± 0.20

7 ACKNOWLEDGEMENTS

We warmly thank the anonymous referee for his thorough reading and questions. FB is indebted to James S. Dunlop for his advice, and also for the economic support for MM during her visit to the University of Edinburgh. The IA Thematic Line *"The assembly history of galaxies resolved in space and time"* is acknowledged for inviting IT for his visit to the Observatory of Lisbon. We gratefully thank Esther Mármol-Queraltó, Ross McLure, Jesús Falcón-Barroso, Francesco La Barbera, Anton Koekemoer, Hugo Messias and Alexandre Vazdekis and for their help through different stages of this project. José Sabater, Britton Smith and Jovan Veljanoski are very much acknowledged for very valuable computational assistance. We have extensively used the following software packages: TOPCAT (Taylor 2005), ALADIN (Bonnarel et al. 2000) and the IDL routines `mpfit` and `mpfitfun` (Markwardt 2009). FB acknowledges the support of the European Research Council via the award of an Advanced Grant to James S. Dunlop, the funding from the ASTRODEEP FP7 programme and the support by FCT via the postdoctoral fellowship SFRH/BPD/103958/2014. This work is supported by Fundao para a Cincia e a Tecnologia (FCT) through national funds (UID/FIS/04434/2013) and by FEDER through COMPETE2020 (POCI-01-0145-FEDER-007672). FB and IT also acknowledges support from grant AYA2013-48226-C3-1-P from the Spanish Ministry of Economy and Competitiveness (MINECO). ECL would like to acknowledge financial support from the ERC via an Advanced Grant under grant agreement no. 321323-NEOGAL. APC acknowledges a COFUND/Durham Junior Research Fellowship under EU grant [267209]. PGP-G acknowledges support from Spanish Government Grants AYA2012-31277 and AYA2015-70815-ERC. This work has made use of the Rainbow Cosmological Surveys Database, which is operated by the Universidad Complutense de Madrid (UCM), partnered with the University of California Observatories at Santa Cruz (UCO/Lick,UCSC).

REFERENCES

- Arnouts S., Cristiani S., Moscardini L., Matarrese S., Lucchin F., Fontana A., Giallongo E., 1999, *MNRAS*, 310, 540
- Atkinson A. M., Abraham R. G., Ferguson A. M. N., 2013, *ApJ*, 765, 28
- Barro G. et al., 2011a, *ApJS*, 193, 13
- Barro G. et al., 2011b, *ApJS*, 193, 30
- Barro G. et al., 2013, *ApJ*, 765, 104
- Beckwith S. V. W. et al., 2006, *AJ*, 132, 1729
- Bell E. F., McIntosh D. H., Katz N., Weinberg M. D., 2003, *ApJS*, 149, 289
- Bell E. F. et al., 2006, *ApJ*, 640, 241
- Bell E. F. et al., 2012, *ApJ*, 753, 167
- Bertin E., Arnouts S., 1996, *A&AS*, 117, 393
- Bezanson R., van Dokkum P. G., Tal T., Marchesini D., Kriek M., Franx M., Coppi P., 2009, *ApJ*, 697, 1290
- Blanton M. R. et al., 2005, *AJ*, 129, 2562
- Bluck A. F. L., Conselice C. J., Buitrago F., Grützbauch R., Hoyos C., Mortlock A., Bauer A. E., 2012, *ApJ*, 747, 34
- Bonnarel F. et al., 2000, *A&AS*, 143, 33
- Bouwens R. J. et al., 2012, *ApJ*, 752, L5
- Boylan-Kolchin M., Springel V., White S. D. M., Jenkins A., Lemson G., 2009, *MNRAS*, 398, 1150
- Bruce V. A. et al., 2012, *MNRAS*, 427, 1666
- Bruzual G., Charlot S., 2003, *MNRAS*, 344, 1000
- Buitrago F., Trujillo I., Conselice C. J., Bouwens R. J., Dickinson M., Yan H., 2008, *ApJ*, 687, L61
- Buitrago F., Trujillo I., Conselice C. J., Häußler B., 2013, *MNRAS*, 428, 1460
- Cassata P. et al., 2010, *ApJ*, 714, L79
- Cassata P. et al., 2011, *ApJ*, 743, 96
- Ceverino D., Dekel A., Tweed D., Primack J., 2015, *MNRAS*, 447, 3291
- Chabrier G., 2003, *PASP*, 115, 763
- Cimatti A. et al., 2008, *A&A*, 482, 21
- Coccato L., Gerhard O., Arnaboldi M., 2010, *MNRAS*, 407, L26
- Cole S., Lacey C. G., Baugh C. M., Frenk C. S., 2000, *MNRAS*, 319, 168
- Conselice C. J., 2006, *ApJ*, 638, 686
- Conselice C. J., Yang C., Bluck A. F. L., 2009, *MNRAS*, 394, 1956
- Cooper A. P., D'Souza R., Kauffmann G., Wang J., Boylan-Kolchin M., Guo Q., Frenk C. S., White S. D. M., 2013, *MNRAS*, 434, 3348
- Crnojević D., Ferguson A. M. N., Irwin M. J., Bernard E. J., Arimoto N., Jablonka P., Kobayashi C., 2013, *MNRAS*, 432, 832
- Croom S. M., Smith R. J., Boyle B. J., Shanks T., Loaring N. S., Miller L., Lewis I. J., 2001, *MNRAS*, 322, L29
- Croton D. J. et al., 2006, *MNRAS*, 365, 11
- Daddi E. et al., 2005, *ApJ*, 626, 680
- Damjanov I. et al., 2009, *ApJ*, 695, 101
- de Jong R. S., 2008, *MNRAS*, 388, 1521

- D'Souza R., Kauffman G., Wang J., Vegetti S., 2014, *MNRAS*, 443, 1433
- Duc P. A. et al., 2015, *MNRAS*, 446, 120
- Ellis R. S. et al., 2013, *ApJ*, 763, L7
- Falcón-Barroso J. et al., 2006, *New A Rev.*, 49, 515
- Ferré-Mateu A., Vazdekis A., de la Rosa I. G., 2013, *MNRAS*, 431, 440
- Ferreras I. et al., 2014, *MNRAS*, 444, 906
- Fumagalli M. et al., 2014, *ApJ*, 796, 35
- Giavalisco M., Livio M., Bohlin R. C., Macchetto F. D., Stecher T. P., 1996, *AJ*, 112, 369
- Guo Q. et al., 2011, *MNRAS*, 413, 101
- Hopkins P. F., Bundy K., Murray N., Quataert E., Lauer T. R., Ma C. P., 2009, *MNRAS*, 398, 898
- Huang S., Ho L. C., Peng C. Y., Li Z. Y., Barth A. J., 2013, *ApJ*, 768, L28
- Huertas-Company M. et al., 2013, *MNRAS*, 428, 1715
- Ilbert O. et al., 2006, *A&A*, 457, 841
- Kaviraj S., 2010, *MNRAS*, 406, 382
- Khochfar S., Silk J., 2006, *ApJ*, 648, L21
- Koekemoer A. M. et al., 2013, *ApJS*, 209, 3
- Kormendy J., Fisher D. B., Cornell M. E., Bender R., 2009, *ApJS*, 182, 216
- Krajnović D. et al., 2008, *MNRAS*, 390, 93
- Krajnović D. et al., 2013, *MNRAS*, 432, 1768
- Krist J., 1995, in R. A. Shaw, H. E. Payne, & J. J. E. Hayes, ed., *Astronomical Data Analysis Software and Systems IV. Astronomical Society of the Pacific Conference Series*, Vol. 77, p. 349
- La Barbera F., Ferreras I., de Carvalho R. R., Bruzual G., Charlot S., Pasquali A., Merlin E., 2012, *MNRAS*, 426, 2300
- La Barbera F., Ferreras I., Vazdekis A., de la Rosa I. G., de Carvalho R. R., Trevisan M., Falcón-Barroso J., Ricciardelli E., 2013, *MNRAS*, 433, 3017
- Le Fèvre O. et al., 2005, *A&A*, 439, 845
- López-Sanjuan C. et al., 2012, *A&A*, 548, A7
- Lotz J. M., Jonsson P., Cox T. J., Primack J. R., 2008, *MNRAS*, 391, 1137
- Markwardt C. B., 2009, in D. A. Bohlender, D. Durand, & P. Dowler, ed., *Astronomical Data Analysis Software and Systems XVIII. Astronomical Society of the Pacific Conference Series*, Vol. 411, pp. 251–+
- Mármol-Queraltó E., Trujillo I., Pérez-González P. G., Varela J., Barro G., 2012, *MNRAS*, 422, 2187
- Mármol-Queraltó E., Trujillo I., Villar V., Barro G., Pérez-González P. G., 2013, *MNRAS*, 429, 792
- Martín-Navarro I. et al., 2015, *ApJ*, 798, L4
- Martínez-Delgado D. et al., 2010, *AJ*, 140, 962
- McLure R. J. et al., 2013, *MNRAS*, 432, 2696
- Newman A. B., Ellis R. S., Bundy K., Treu T., 2012, *ApJ*, 746, 162
- Oke J. B., Gunn J. E., 1983, *ApJ*, 266, 713
- Oser L., Ostriker J. P., Naab T., Johansson P. H., Burkert A., 2010, *ApJ*, 725, 2312
- Peng C. Y., Ho L. C., Impey C. D., Rix H. W., 2010, *AJ*, 139, 2097
- Pérez-González P. G., Trujillo I., Barro G., Gallego J., Zamorano J., Conselice C. J., 2008a, *ApJ*, 687, 50
- Pérez-González P. G. et al., 2008b, *ApJ*, 675, 234
- Pirzkal N. et al., 2005, *ApJ*, 622, 319
- Purcell C. W., Bullock J. S., Zentner A. R., 2007, *ApJ*, 666, 20
- Ravikumar C. D. et al., 2007, *A&A*, 465, 1099
- Rejkuba M., Harris W. E., Greggio L., Harris G. L. H., Jerjen H., Gonzalez O. A., 2014, *ApJ*, 791, L2
- Ribeiro B. et al., 2016, *A&A*, 593, A22
- Ricciardelli E., Trujillo I., Buitrago F., Conselice C. J., 2010, *MNRAS*, 406, 230
- Ricciardelli E., Vazdekis A., Cenarro A. J., Falcón-Barroso J., 2012, *MNRAS*, 424, 172
- Roediger J. C., Courteau S., 2015, *MNRAS*, 452, 3209
- Ruiz P., Trujillo I., Mármol-Queraltó E., 2015, *MNRAS*, 454, 1605
- Salpeter E. E., 1955, *ApJ*, 121, 161
- Sandin C., 2014, *A&A*, 567, A97
- Sandin C., 2015, *A&A*, 577, A106
- Szomoru D., Franx M., van Dokkum P. G., 2012, *ApJ*, 749, 121
- Tal T., van Dokkum P. G., 2011, *ApJ*, 731, 89
- Tal T., van Dokkum P. G., Nelan J., Bezanson R., 2009, *AJ*, 138, 1417
- Taylor M. B., 2005, in P. Shopbell, M. Britton, R. Ebert, eds, *Astronomical Data Analysis Software and Systems XIV. Astronomical Society of the Pacific Conference Series*, Vol. 347, p. 29
- Toft S. et al., 2007, *ApJ*, 671, 285
- Trujillo I., Bakos J., 2013, *MNRAS*, 431, 1121
- Trujillo I., Fliri J., 2016, *ApJ*, 823, 123
- Trujillo I., Conselice C. J., Bundy K., Cooper M. C., Eisenhardt P., Ellis R. S., 2007, *MNRAS*, 382, 109
- Trujillo I., Ferreras I., de La Rosa I. G., 2011, *MNRAS*, 415, 3903
- Trujillo I., Ferré-Mateu A., Balcells M., Vazdekis A., Sánchez-Blázquez P., 2014, *ApJ*, 780, L20
- Trujillo I. et al., 2006a, *MNRAS*, 373, L36
- Trujillo I. et al., 2006b, *ApJ*, 650, 18
- van der Wel A. et al., 2014, *ApJ*, 788, 28
- van Dokkum P. G., 2005, *AJ*, 130, 2647
- van Dokkum P. G., Abraham R., Merritt A., 2014, *ApJ*, 782, L24
- van Dokkum P. G. et al., 2010, *ApJ*, 709, 1018
- Vanzella E. et al., 2005, *A&A*, 434, 53
- Vazdekis A., Ricciardelli E., Cenarro A. J., Rivero-González J. G., Díaz-García L. A., Falcón-Barroso J., 2012, *MNRAS*, 424, 157
- Wellons S. et al., 2016, *MNRAS*, 456, 1030
- Williams C. C. et al., 2014, *ApJ*, 780, 1
- Xie L., Guo Q., Cooper A. P., Frenk C. S., Li R., Gao L., 2015, *MNRAS*, 447, 636
- Zackrisson E., Bergvall N., Östlin G., Micheva G., Leksell M., 2006, *ApJ*, 650, 812
- Zibetti S., Ferguson A. M. N., 2004, *MNRAS*, 352, L6
- Zibetti S., White S. D. M., Brinkmann J., 2004, *MNRAS*, 347, 556
- Zolotov A. et al., 2015, *MNRAS*, 450, 2327

APPENDIX A: H-BAND PROFILES

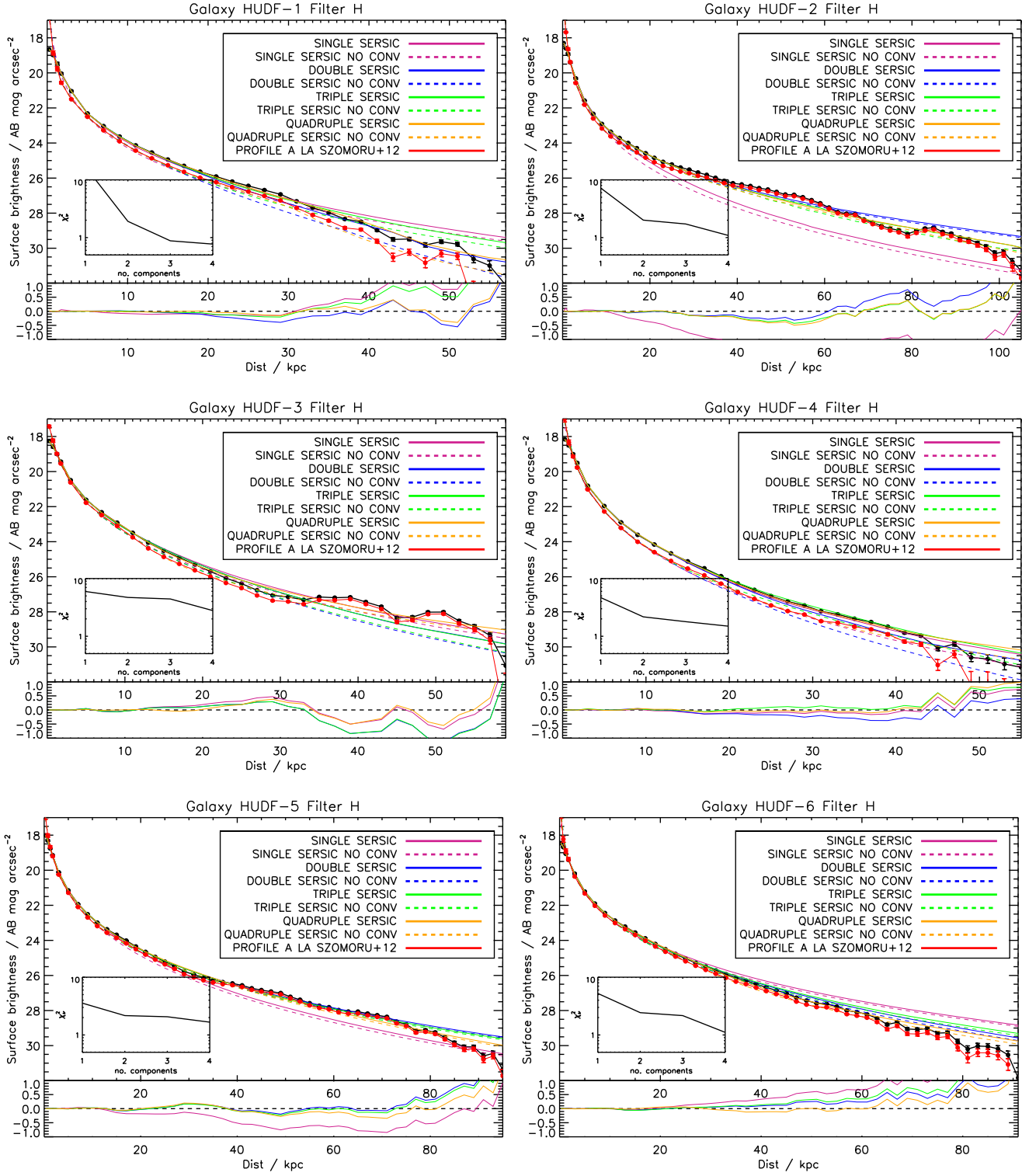


Figure A1. Observed (black line), model (convolved and non-convolved with the PSF, coloured solid and dashed lines respectively, with colours indicated in the legend) and “a la Szomoru” (deconvolved adding the residuals of the 4 Sérsic fit; red line) galaxy surface brightness profiles for our galaxy sample in the H-band. The subplot shows the reduced chi-square (χ^2_r) values for the Sérsic fits we performed. The bottom miniplots display the differences between the observed surface brightness profile and the multi-Sérsic PSF convolved models.